Article

Discovery Medicine 2025; 37(201): 2475–2487
https://doi.org/10.24976/Discov.Med.202537201.208

LGR4 Promotes Lung Adenocarcinoma Progression via Activation of the NF-κB Signaling Pathway

Lu Li[1], Chengcheng Yang[1], Xiaowen Kang[1], Zhaoguo Li[1], Kun Huang[1], Wei Zhang[2,*]

[1]Department of Pulmonary and Critical Care Medicine, The Second Affiliated Hospital of Harbin Medical University, 150086 Harbin, Heilongjiang, China
[2]Department of Pulmonary and Critical Care Medicine, The First Affiliated Hospital of Harbin Medical University, 150001 Harbin, Heilongjiang, China
*Correspondence: weipoza@163.com (Wei Zhang)
Submitted: 9 July 2025 Revised: 16 September 2025 Accepted: 22 September 2025 Published: 20 October 2025

Background: Lung adenocarcinoma (LUAD) is a major cause of cancer-related mortality worldwide. However, its key driver genes and molecular mechanisms remain insufficiently defined. This study aimed to identify novel oncogenic drivers in LUAD, focusing on leucine-rich repeat-containing G protein-coupled receptor 4 (LGR4). We analyzed transcriptomic data from The Cancer Genome Atlas (TCGA) and developed a prognostic model.

Methods: Differentially expressed genes between LUAD and normal lung tissues were identified using TCGA data. An initial analysis using DESeq2 with a fold-change threshold of $\geq$4 identified 3100 significantly differentially expressed genes (adjusted $p < 0.05$; 2671 upregulated and 429 downregulated). Univariate Cox regression (hazard ratio, HR) and least absolute shrinkage and selection operator (LASSO) regression were employed to construct a prognostic risk model, reducing the pool to 28 prognostic genes. Intersecting these with 19 genes both highly expressed and associated with poor prognosis yielded 10 key prognostic markers, including LGR4. Experimental validation was performed: *LGR4* mRNA expression was quantified by quantitative reverse transcription polymerase chain reaction (RT-qPCR) in clinical LUAD samples, and functional assays (cell counting kit-8 (CCK-8) proliferation, wound healing, and Transwell migration/invasion) as well as a nude mouse xenograft model were performed to assess the role of LGR4.

Results: *In vitro* assays demonstrated that *LGR4* knockdown significantly suppressed proliferation, migration, and invasion of A549 and H1650 cells (all $p < 0.05$), whereas *LGR4* overexpression in H1299 cells produced the opposite effect ($p < 0.05$). *In vivo*, a subcutaneous xenograft model in nude mice further confirmed that *LGR4* promotes tumor growth ($p < 0.05$). Mechanistic analyses revealed that *LGR4* activates the nuclear factor kappa-B (NF-κB) signaling pathway, leading to the upregulation of cyclin D1 (*CCND1*), matrix metalloproteinase 2 (*MMP2*), and vascular endothelial growth factor (*VEGF*) ($p < 0.05$), which regulate cell cycle progression, extracellular matrix remodeling, and angiogenesis, thereby facilitating LUAD progression.

Conclusion: Collectively, these findings demonstrate that LGR4 serves as a novel prognostic biomarker and potential therapeutic target in LUAD. This study provides a theoretical framework for further elucidating the molecular mechanisms underlying lung adenocarcinoma and advancing targeted therapeutic strategies.

Keywords: lung adenocarcinoma; LGR4; differential gene expression; prognostic risk model; NF-κB signaling pathway; tumor progression; targeted therapy

Introduction

Lung adenocarcinoma (LUAD) is one of the most prevalent subtypes of lung cancer, with an incidence rate that has continued to rise in recent years [1–4]. Because early-stage LUAD often lacks obvious clinical symptoms, many patients are diagnosed at advanced stages, leading to poor overall prognosis. Despite significant advances in surgical resection, radiotherapy, chemotherapy, and targeted therapies, overall survival outcomes remain unsatisfactory [5]. Therefore, identifying novel molecular mechanisms and potential therapeutic targets is essential to improve clinical management and patient outcomes.

Recent investigations into the tumor microenvironment, signaling pathways, and prognostic biomarkers have provided valuable insights into the complex molecular regulatory networks underlying tumorigenesis and disease progression [6,7]. Numerous studies have demonstrated that aberrant activation of specific signaling pathways is strongly associated with key tumor biological behaviors, including proliferation, migration, invasion, and drug resistance [8,9]. For example, the nuclear factor kappa-B (NF-κB) signaling pathway, which plays a pivotal role in regulating inflammation and cell survival, has been implicated in tumor progression across multiple malignancies [10–15]. Furthermore, advances in high-throughput sequencing and large-scale bioinformatics analyses have facilitated

the identification of differentially expressed genes and the prognostic model, thereby deepening our understanding of tumor pathophysiology.

Leucine-rich repeat-containing G protein-coupled receptor 4 (*LGR4*), a member of the G protein-coupled receptor family, has recently attracted considerable attention due to its abnormal expression and functional significance in multiple cancers [8,9,16–21]. Previous studies have shown that LGR4 promotes tumor progression by regulating cell cycle progression, migration, and stemness maintenance in malignancies such as breast and prostate cancers. However, its expression profile, clinical relevance, and potential molecular mechanisms in LUAD remain unclear. Notably, whether LGR4 regulates LUAD cell proliferation, migration, and invasion through interaction with key signaling pathways such as NF-κB requires further investigation [8,16,22,23].

This study aimed to systematically investigate the biological function and molecular mechanisms of LGR4 in LUAD. We hypothesize that LGR4 is upregulated in LUAD and exerts pro-tumorigenic effects by activating the NF-κB signaling pathway, thereby promoting tumor cell proliferation, migration, and invasion. If validated, the findings from this study will not only provide novel insights into LUAD pathogenesis but also identify potential prognostic biomarkers and therapeutic targets for clinical application.

Materials and Methods

Data Acquisition and Differential Expression Analysis

Transcriptomic profiles and corresponding clinical information for LUAD were retrieved from The Cancer Genome Atlas (TCGA) via the Genomic Data Commons (GDC) portal (https://portal.gdc.cancer.gov). Raw count data were normalized using the DESeq2 package version 1.38.3 (Bioconductor Project, Seattle, WA, USA). Differentially expressed genes (DEGs) between LUAD and adjacent normal lung tissues were identified with DESeq2, applying a cutoff of $|\log_2 FC| \geq 2$ (fold change ≥ 4) and an adjusted p-value < 0.05.

Functional Enrichment Analysis

Gene Ontology (GO) and Kyoto Encyclopedia of Genes and Genomes (KEGG) pathway enrichment analyses were performed on DEGs using the *clusterProfiler* R package version 4.2.0 (Bioconductor Project, Seattle, WA, USA) to determine their biological significance. Gene Set Variation Analysis (GSVA) was performed to compare pathway activity differences between LGR4-high and LGR4-low expression groups.

Survival Analysis and Prognostic Model Construction

Univariate Cox regression (hazard ratios, HR) was used to identify survival-associated genes among the DEGs. The optimal lambda for least absolute shrinkage and selection operator (LASSO) Cox regression was determined through cross-validation, and a multivariate Cox model adjusting for clinical covariates (e.g., age and tumor stage) was also evaluated. Kaplan–Meier survival curves with log-rank tests were employed to validate the prognostic significance of candidate genes.

Clinical Sample Collection and RT-qPCR Validation

Paired LUAD and adjacent non-tumor tissues (n = 9) were collected with informed consent and ethical approval. Total RNA was extracted and reverse-transcribed into cDNA. LGR4 mRNA expression was quantified using quantitative reverse transcription polymerase chain reaction (RT-qPCR), with glyceraldehyde 3-phosphate dehydrogenase (GAPDH) as an internal control. The following primer sequences were used: *LGR4* (F: 5′-TTGTGGGCAACTTCAAGCTG-3′; R: 5′-AACCCCAAAATGCACAGCAC-3′) and *GAPDH* (F: 5′-GAAGGTGAAGGTCGGAGTCA-3′; R: 5′-GAAGATGGTGATGGGATTTC-3′). Each reaction was performed in triplicate, and relative expression was calculated using the $2^{-\Delta\Delta Ct}$ method. Written informed consent was obtained from all participants prior to sample collection. This study was approved by the Medical Ethics Committee of Institution (Human Ethics Approval No. KY2023-139).

Cell Culture and Transfection

Human LUAD cell lines A549 (ATCC CCL-185™), NCI-H1650 (ATCC CRL-5883™), NCI-H1299 (ATCC CRL-5803™) were cultured in RPMI-1640 medium, while PC-9 (ATCC CRL-5925™), and normal human bronchial epithelial cells (HBE; ATCC PCS-300-010™) were cultured in DMEM. All media were supplemented with 10% fetal bovine serum (FBS). All cell lines were obtained from ATCC and authenticated by short tandem repeat (STR) profiling and verified to be mycoplasma-free. The incubation conditions set in the incubator were as follows: the temperature was maintained at 37 °C, and the carbon dioxide concentration inside the incubator was controlled at 5%. For LGR4 silencing, cells were transfected with small interfering RNAs (siRNAs) targeting LGR4 (RiboBio, Guangzhou, China). The antisense sequences were as follows: siRNA-1, 5′-CCUUAAAGAGCUAGGAUUU-3′; siRNA-2, 5′-CCUGAUAUCUCUAAGGAUU-3′; siRNA-3, 5′-GGAGAAAGGUACUGCUGAU-3′.

A non-targeting siRNA duplex (siNC; sense: 5′-UUCUCCGAACGUGUCACGUTT-3′) served as the negative control. For knockdown experiments, cells were transfected with 50 nM siRNA or 2 μg shRNA plasmid

using Lipofectamine 3000 (Cat. No. L3000008, Thermo Fisher Scientific, Waltham, MA, USA). Functional assays were performed 48 hours post-transfection. For *LGR4* overexpression experiments, cells were transfected with 2 µg of the pcDNA3.1-LGR4 plasmid, while the empty pcDNA3.1 vector was used as a control. Transfection efficiency was verified by RT-qPCR and western blotting.

Cell Proliferation, Migration, and Invasion Assays

For proliferation assays, cells were seeded into 96-well plates (2000 cells/well), and viability was measured at 0, 24, 48, 72 and 96 hours using a cell counting kit-8 (CCK-8) (Cat. No. C0037, Beyotime Biotechnology, Shanghai, China) following the manufacturer's instructions. Absorbance was recorded at 450 nm. Wound healing assays were performed by creating a scratch in confluent monolayers and monitoring gap closure over 24 hours, with images captured at 0 and 24 hours. For Transwell migration and invasion assays, 8-µm pore inserts (Corning Inc., Corning, NY, USA) were used; 5×10^4 cells were seeded in the upper chamber in serum-free medium, while medium supplemented with 10% FBS was placed in the lower chamber. After 24 hours, migrated or invaded cells on the underside were fixed, stained with crystal violet, and quantified under a microscope (ECLIPSE Ts2R, Nikon Corporation, Tokyo, Japan). All assays were performed in $\geq$3 biological replicates.

In Vivo Tumorigenicity Assay

Female BALB/c nude mice (6–8 weeks old; n = 6 per group) were anesthetized with isoflurane (3% induction) and euthanized by cervical dislocation under anesthesia. LGR4-knockdown A549 cells or LGR4-overexpressing H1299 cells (1×10^6 cells in 100 µL phosphate-buffered saline (PBS)) were injected subcutaneously into the flank of each mouse. Tumor volume and mouse body weight were measured every 3 days, with tumor volume calculated as $\frac{1}{2} \times \text{length} \times \text{width}^2$. After 4 weeks, mice were sacrificed, and tumors were excised, photographed, and weighed. Representative tumor images were recorded. Tumor tissues were fixed, paraffin-embedded, and subjected to immunohistochemistry (IHC). All animal experiments were conducted in compliance with the Chinese Animal License Regulations and were approved by the Animal Care and Use Committee of the Second Affiliated Hospital of Harbin Medical University (Animal Ethics Approval No. SYDW2023-087).

RNA Sequencing and NF-κB Pathway Validation

Total RNA from *LGR4*-knockdown and control A549 cells was sequenced on the Illumina platform (NovaSeq 6000, Illumina, Inc., San Diego, CA, USA). Reads were aligned, counted, and analyzed with DESeq2 for differential expression. Count data were $\log_2$-transformed and normalized, and batch effects were corrected using standard methods (e.g., ComBat, details not specified). Gene set enrichment analysis identified enrichment of the NF-κB signaling pathway.

To validate the findings, western blotting was performed. Cells were harvested 48 hours post-treatment, washed with cold PBS, and lysed on ice for 30 minutes in radio immunoprecipitation assay (RIPA) buffer containing protease and phosphatase inhibitors. Lysates were centrifuged at 14,000 ×g for 15 minutes at 4 °C, and the supernatant was collected. Protein concentrations were determined using a bicinchoninic acid (BCA) assay kit (Cat. No. 23227, Thermo Scientific, Waltham, MA, USA). Equal amounts (20–30 µg) of protein were separated on 10–12% sodium dodecyl sulfate-polyacrylamide gel electrophoresis (SDS-PAGE) gels and transferred to polyvinylidene fluoride (PVDF) membranes at 100 V for 90 minutes. Membranes were blocked in 5% bovine serum albumin (BSA) for 1 hour at room temperature, incubated overnight at 4 °C with primary antibodies (e.g., p65, GAPDH; 1:1000), washed three times in TBS with Tween-20 (TBST), and incubated with horseradish peroxidase (HRP)-conjugated secondary antibodies (1:5000) for 1 hour. Bands were visualized with enhanced chemiluminescence (ECL) reagent (Cat. No. 32106; Thermo Fisher Scientific, Waltham, MA, USA) and imaged. Band intensities were quantified using ImageJ 1.52j (National Institutes of Health, Bethesda, MD, USA) and normalized to GAPDH.

Primary antibodies included p65 (rabbit mAb, 1:1000; Cat. No. 8242, Cell Signaling Technology), phospho-p65 Ser536 (rabbit mAb, 1:1000; Cat. No. 3033, Cell Signaling Technology), IκBα (rabbit mAb, 1:1000; Cat. No. 4814, Cell Signaling Technology), phospho-IκBα Ser32 (rabbit mAb, 1:1000; Cat. No. 2859, Cell Signaling Technology), IKKα/β (rabbit Ab, 1:1000; Cat. No. 2697, Cell Signaling Technology), phospho-IKKα/β (Ser176/180; rabbit, 1:1000; Cat. No. 2697, Cell Signaling Technology), CCND1 (mouse mAb, 1:500; Cat. No. 2978, Cell Signaling Technology), MMP2 (rabbit mAb, 1:1000; Cat. No. 40994, Cell Signaling Technology), vascular endothelial growth factor (VEGF) (rabbit mAb, 1:1000; Cat. No. 65373, Cell Signaling Technology), and GAPDH (rabbit mAb, 1:5000; Cat. No. 5174, Cell Signaling Technology). Secondary antibodies were goat anti-rabbit IgG-HRP (1:5000; Cat. No. 31460, Thermo Fisher Scientific) and goat anti-mouse IgG-HRP (1:5000; Cat. No. 31430, Thermo Fisher Scientific).

Signal was developed using ECL Detection Reagent and analyzed by ImageJ. Secondary HRP-conjugated antibodies were used and bands were detected by ECL. Pyrrolidine dithiocarbamate (PDTC, 100 µM) was applied as an NF-κB inhibitor. Cells were treated for 24 hours before subsequent assays.

Immunohistochemistry (IHC)

Paraffin-embedded tissue sections (4 µm) were deparaffinized in xylene, rehydrated through graded ethanol, and subjected to antigen retrieval in citrate buffer (pH 6.0) using microwave heating for 10 minutes. Sections were incubated with 3% H_2O_2 for 20 minutes to quench endogenous peroxidase activity, followed by blocking with 5% BSA for 30 minutes. Slides were incubated overnight at 4 °C with anti-Ki-67 antibody (1:200), washed, and incubated with HRP-conjugated secondary antibody for 45 minutes at room temperature. 33′-diaminobenzidine (DAB) was applied for chromogenic detection (2–5 minutes), followed by hematoxylin counterstaining for 1 minute. After dehydration and mounting, images (Leica Microsystems GmbH, Germany) were captured with a 50 µm scale bar, and staining was quantified by Hscore (intensity 0–3 × percentage of positive cells).

Statistical Analysis

Data were presented as mean ± standard deviation (SD). Comparisons between two groups were performed using unpaired Student's *t*-test or Wilcoxon signed-rank test, and among multiple groups by one-way analysis of variance (ANOVA) followed by post hoc tests. Survival analysis was conducted using the log-rank test. Statistical analyses were performed using GraphPad Prism 10 (GraphPad Software, LLC, San Diego, CA, USA) and SPSS 20 (IBM Corp., Armonk, NY, USA). Statistical significance was represented in figures as $p < 0.05$, $p < 0.01$, $p < 0.001$, $p < 0.0001$; "ns" indicated not significant. All comparisons were conducted relative to the baseline group (control or adjacent normal).

Results

Screening and Functional Annotation of Differentially Expressed Genes in Lung Adenocarcinoma

To further characterize expression differences between LUAD and adjacent normal lung tissues, we extracted tumor samples and corresponding normal tissues from the TCGA database and repeated differential expression analysis using DESeq2. With a fold-change threshold of ≥4, 3100 significantly differentially expressed genes were identified, including 2671 upregulated and 429 downregulated genes (**Supplementary Fig. 1A,B**).

Gene Ontology (GO) enrichment analysis was then performed to investigate the biological significance of these DEGs. Results showed that, within Biological Processes, genes were primarily enriched in humoral immune response, immunoglobulin-mediated immune responses, and B cell-mediated immune responses. In terms of molecular function, enrichment was observed in immune receptor activation, antigen binding, and G protein-coupled receptor activation. For cellular components, genes were significantly enriched in immune complexes, collagen, and the extracellular matrix (Fig. 1A,B), highlighting their central role in immune regulation and shaping the tumor microenvironment.

Furthermore, univariate Cox regression analysis was used to evaluate the correlation between differentially expressed genes and patient survival, identifying 88 genes significantly associated with prognosis. Among these, 19 genes correlated with poor prognosis (HR >1), while 69 were linked to longer survival (HR <1) (**Supplementary Fig. 1C**). LASSO regression was applied to refine the prognostic panel, reducing it to 28 candidate genes for constructing a LUAD mortality risk prediction model (Fig. 1C). By intersecting these 28 model genes with the 19 previously identified high-expression poor prognosis genes, 10 key prognostic markers were identified, including LGR4. RT-qPCR validation further confirmed significantly elevated *LGR4* expression in tumor tissues (Fig. 1D,E).

LGR4 Expression and Clinical Relevance in Lung Adenocarcinoma

Bioinformatics analysis of the TCGA-LUAD dataset revealed that LGR4 expression was significantly elevated in LUAD tissues compared to adjacent normal tissues (Fig. 2A). Additionally, its expression was positively correlated with lymph node metastasis, tumor–node–metastasis (TNM) stage, and pathological grade (Fig. 2B), suggesting a potential role for LGR4 in tumor progression.

To validate these findings, we collected paired tumor and adjacent normal tissues from nine LUAD patients. RT-qPCR analysis confirmed that LGR4 mRNA levels were significantly elevated in tumor tissues (Fig. 2C). Immunohistochemistry further revealed that LGR4 was primarily localized to the cell membrane and exhibited higher expression in metastatic lymph nodes (Fig. 2D). *In vitro*, LGR4 expression was significantly upregulated in LUAD cell lines (A549, H1650, H1299, PC-9) compared with normal human bronchial epithelial cells (HBE). Among these, A549 and H1650 exhibited the highest expression, while H1299 exhibited relatively lower levels (Fig. 2E,F).

Establishment of LGR4 Knockdown and Overexpression Models in LUAD Cells

To investigate the functional role of LGR4 in LUAD cells, we established LGR4 knockdown models in A549 and H1650 cells using siRNA transfection and LGR4 overexpression models in H1299 cells. RT-qPCR and western blot analyses confirmed effective silencing by si-LGR4-2 and si-LGR4-3, with si-LGR4-3 demonstrating the strongest knockdown efficiency and thus selected for subsequent experiments. Conversely, overexpression of LGR4 in H1299 cells significantly increased both mRNA and protein levels (Fig. 3A–D).

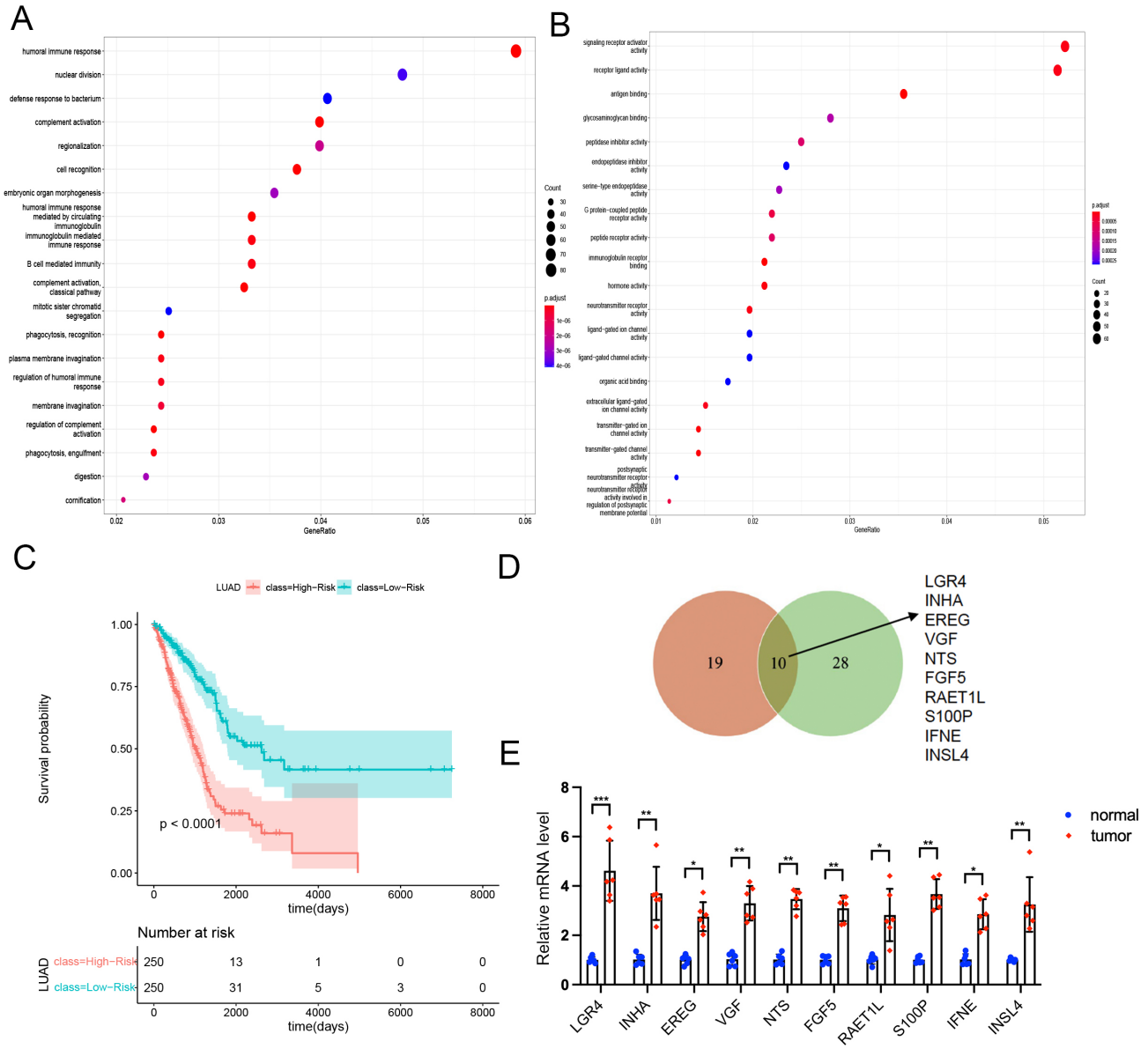

Fig. 1. Screening and functional annotation of differentially expressed genes in lung adenocarcinoma (LUAD). (A,B) Gene Ontology (GO) enrichment analysis of differentially expressed genes (DEGs) in LUAD. The top enriched terms for biological processes, molecular functions, and cellular components are shown. DEGs were significantly associated with immune regulation and tumor microenvironment remodeling. (C) LASSO regression analysis identified 28 prognosis-related genes for constructing a LUAD mortality risk prediction model. (D,E) RT-qPCR validation showing significantly elevated *LGR4* mRNA expression in LUAD tumor tissues compared with adjacent normal tissues. Data are presented as mean ± SD; $*p < 0.05$; $**p < 0.01$; $***p < 0.001$. RT-qPCR, quantitative reverse transcription polymerase chain reaction; *LGR4*, leucine-rich repeat-containing G protein-coupled receptor 4; *INHA*, inhibin subunit alpha; *EREG*, epiregulin; *VGF*, VGF nerve growth factor inducible; *NTS*, neurotensin; *FGF5*, fibroblast growth factor 5; *RAET1L*, retinoic acid early transcript 1L; *S100P*, S100 calcium-binding protein P; *IFNE*, interferon epsilon; *INSL4*, insulin-like 4; LASSO, least absolute shrinkage and selection operator; SD, standard deviation.

LGR4 Regulates LUAD Cell Proliferation

CCK-8 assays demonstrated that LGR4 knockdown significantly suppressed proliferation in A549 and H1650 cells, as indicated by slower growth curves compared with controls (Fig. 4A,B; $***p < 0.001$ at day 4). Conversely, LGR4 overexpression enhanced proliferation rates in H1299 cells (Fig. 4C; $^{###}p < 0.001$). These findings support an oncogenic role of LGR4 in promoting LUAD cell growth.

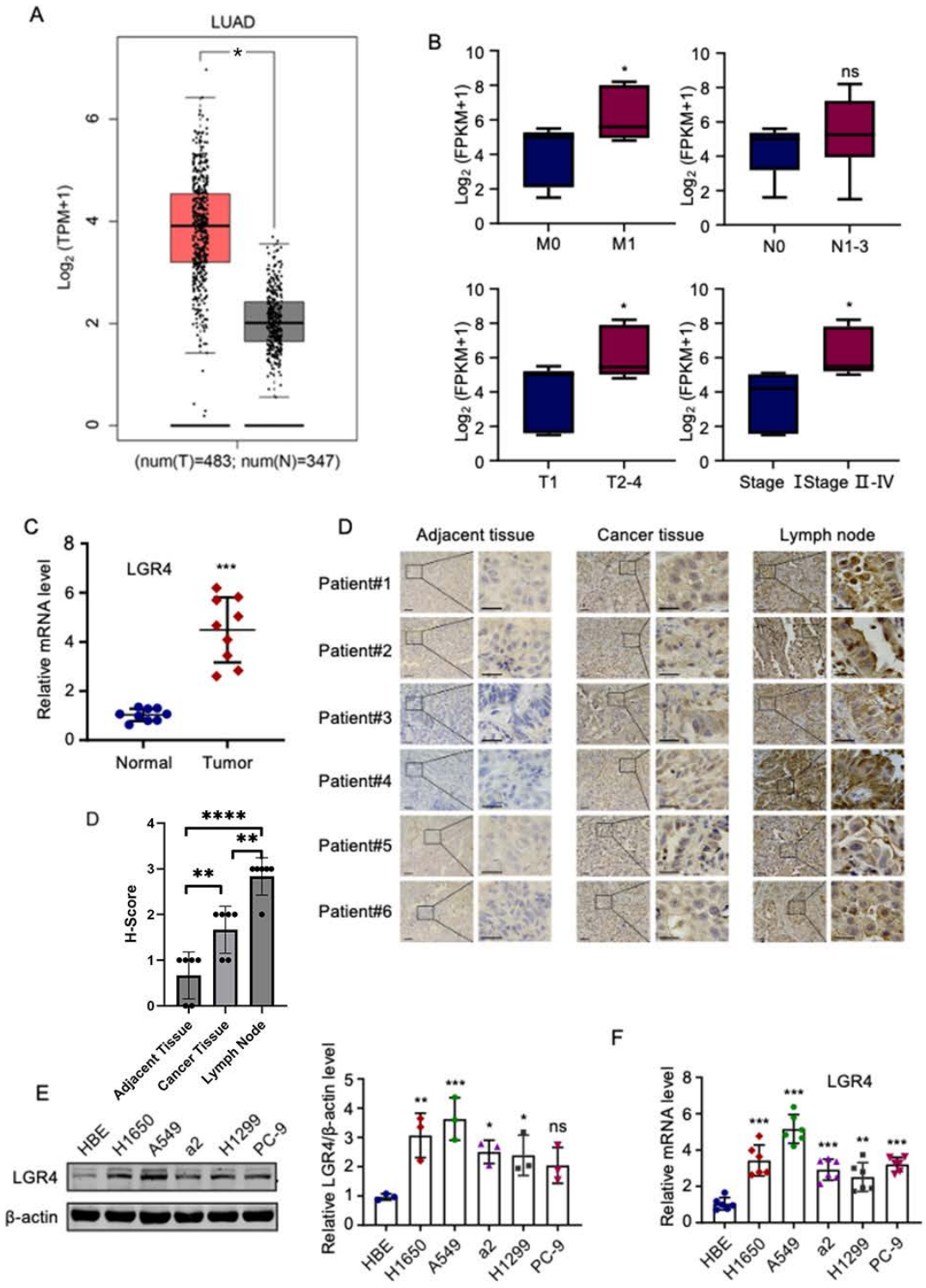

Fig. 2. *LGR4* expression and clinical relevance in LUAD. (A) The Cancer Genome Atlas (TCGA)-LUAD data showing higher *LGR4* expression in tumor tissues compared with normal tissues. (B) *LGR4* expression correlates with advanced tumor–node–metastasis (TNM) stage and lymph node metastasis. (C) RT-qPCR analysis of *LGR4* mRNA levels in tumor versus normal tissues (n = 9). (D) Immunohistochemistry (IHC) showing LGR4 (brown) with predominant membrane localization and higher expression levels in tumor (metastatic lymph node) (scale bar = 50 µm). (E,F) RT-qPCR analysis of *LGR4* in LUAD cell lines versus human bronchial epithelial (HBE) (normal bronchial epithelial) cells. a2: a lung adenocarcinoma cell line, used only for screening purposes and not employed in subsequent experiments. Data are presented as mean ± SD from three replicates; *$p < 0.05$ vs. HBE; **$p < 0.01$; ***$p < 0.001$; ****$p < 0.0001$. TPM, transcripts per million; FPKM, fragments per kilobase of transcript per million mapped reads; H-score, histochemical score; num(T) number of tumor samples; num(N), Number of normal samples; ns, not significant.

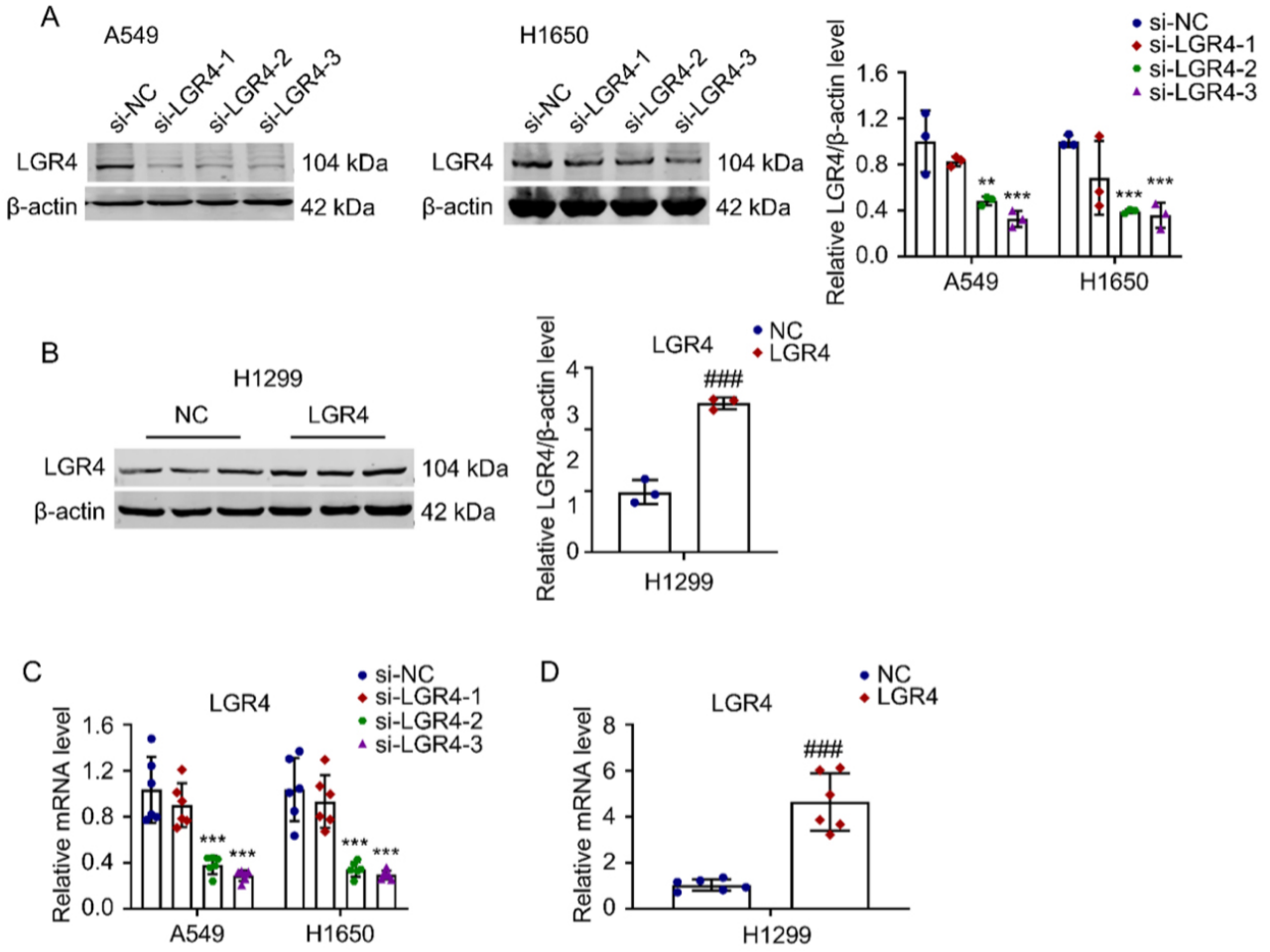

Fig. 3. Establishment of LGR4 knockdown and overexpression models. (A,B) Western blot analysis showing efficient LGR4 knockdown in A549 and H1650 cells using siRNA-3 (***$p < 0.001$ vs. siNC) and successful overexpression in H1299 cells ($^{###}p < 0.001$ vs. vector). (C,D) RT-qPCR analysis of *LGR4* mRNA levels in A549/H1650 cells (si-NC vs. si-LGR4) and H1299 cells (NC vs. LGR4-OE). Data are presented as mean ± SD; **$p < 0.01$; ***$p < 0.001$; $^{###}p < 0.001$. siRNA, small interfering RNA; OE, overexpression; NC, negative control group.

LGR4 Promotes LUAD Cell Migration and Invasion

To evaluate the role of LGR4 in cell motility, wound healing and Transwell assays were performed. In A549 and H1650 cells, LGR4 knockdown significantly reduced wound closure and decreased both migration and invasion compared with controls (Fig. 5A,B; $p < 0.05$). Conversely, in H1299 cells, LGR4 overexpression enhanced wound healing and markedly increased migration and invasion (Fig. 5C,D; $p < 0.05$). Collectively, these findings suggest that LGR4 plays a crucial role in driving LUAD cell motility and invasiveness.

LGR4 Enhances Tumor Growth In Vivo

To validate the *in vitro* findings, a subcutaneous xenograft model was established in nude mice by injecting LGR4-knockdown A549 cells and LGR4-overexpressing H1299 cells. Tumor growth was significantly reduced in the LGR4-knockdown group, whereas LGR4 overexpression markedly accelerated tumor expansion (Fig. 6A–D). Immunohistochemistry further demonstrated weaker Ki67 staining in tumors from the LGR4-knockdown group and stronger Ki67 staining in the LGR4-overexpression group (Fig. 6E,F), supporting the conclusion that LGR4 promotes tumor proliferation *in vivo*.

LGR4 Activates the NF-κB Pathway to Promote LUAD Progression

Western blot analysis revealed that LGR4 overexpression in H1299 cells significantly increased phosphorylation of p65, IκBα, and IKKα/β, while LGR4 knockdown in A549 and H1650 cells reduced phosphorylation of these proteins (Fig. 7A,B). To verify the functional role of NF-κB activation, LGR4-overexpressing cells were treated with the NF-κB inhibitor PDTC (100 μM). PDTC effectively suppressed LGR4-induced NF-κB activation and reversed the enhanced proliferation (Fig. 7C,D; $p < 0.05$). At higher

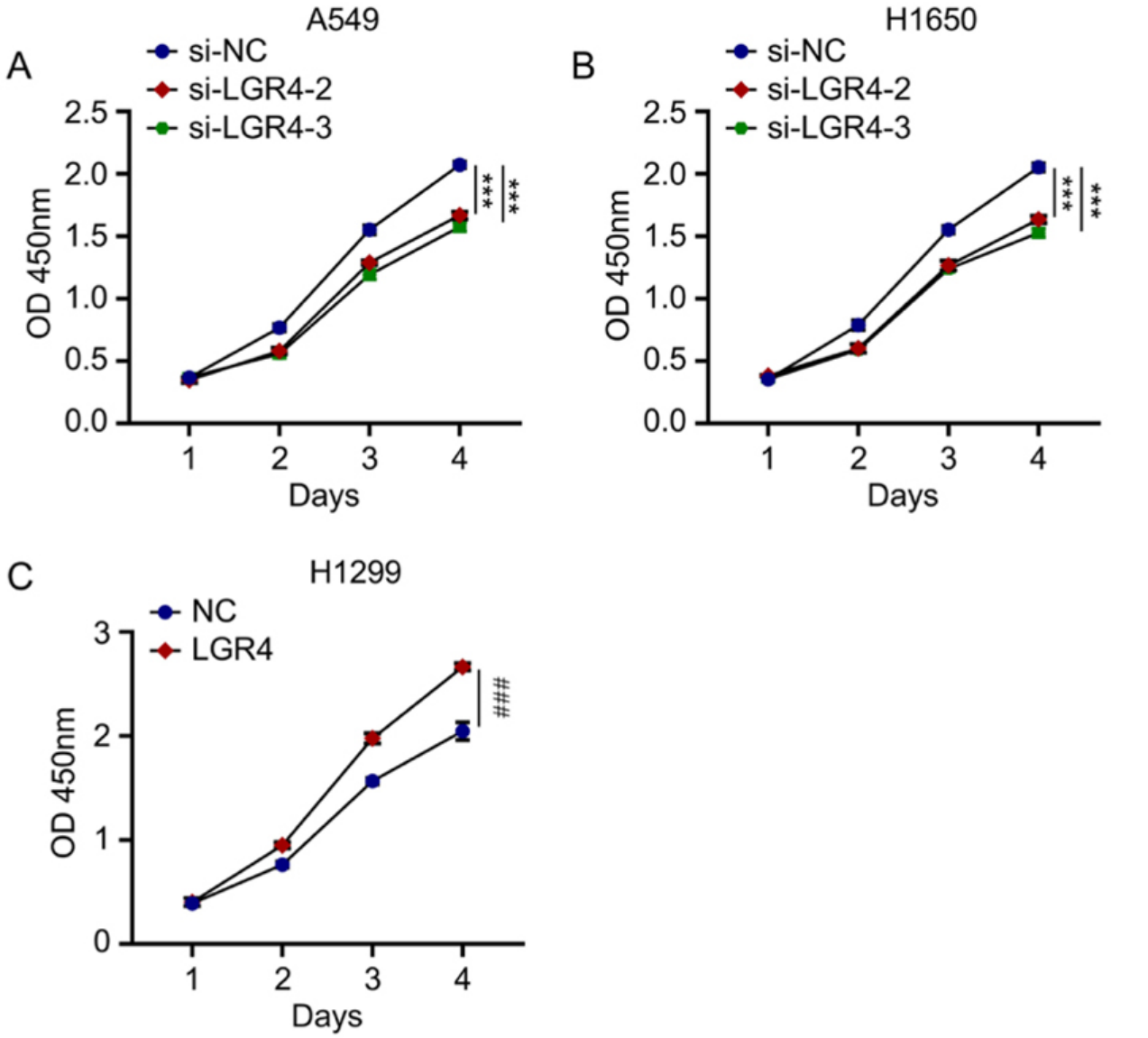

Fig. 4. LGR4 regulates LUAD cell proliferation. (A,B) CCK-8 assays showing that LGR4 knockdown significantly inhibits proliferation in A549 and H1650 cells (***$p < 0.001$ vs. control). (C) LGR4 overexpression promotes proliferation in H1299 cells ($^{###}p < 0.001$ vs. control). Data are presented as mean ± SD from three independent replicates; ***$p < 0.001$; $^{###}p < 0.001$. CCK-8, cell counting kit-8; OD, optical density.

concentrations, PDTC may further suppress the proliferation of LGR4-overexpressing cells via non-specific mechanisms, and when combined with our normalization procedure, this can result in a relative proliferation rate lower than that of untreated H1299 control cells.

Additionally, RT-qPCR showed that *LGR4* overexpression upregulated NF-κB target genes *CCND1*, *MMP2*, and *VEGF*, whereas PDTC treatment reverses these effects (Fig. 7E; $p < 0.05$). Collectively, these findings indicate that *LGR4* promotes LUAD progression at least in part by activating the NF-κB pathway, thereby enhancing *CCND1*, *MMP2*, and *VEGF* expression, leading to accelerated cell cycle progression, ECM degradation, and angiogenesis.

Discussion

This study systematically investigated the role of LGR4 in lung adenocarcinoma and demonstrated that LGR4 is significantly upregulated in tumor tissues compared with normal lung samples, as confirmed by TCGA data and clinical specimen analyses. Elevated LGR4 expression correlated with adverse clinicopathological features, including lymph node metastasis, higher TNM stage, and poorer pathological grade, suggesting that LGR4 may serve as an important prognostic marker and contribute to tumor progression.

In vitro experiments further revealed that LGR4 plays a pivotal role in regulating lung adenocarcinoma cell be-

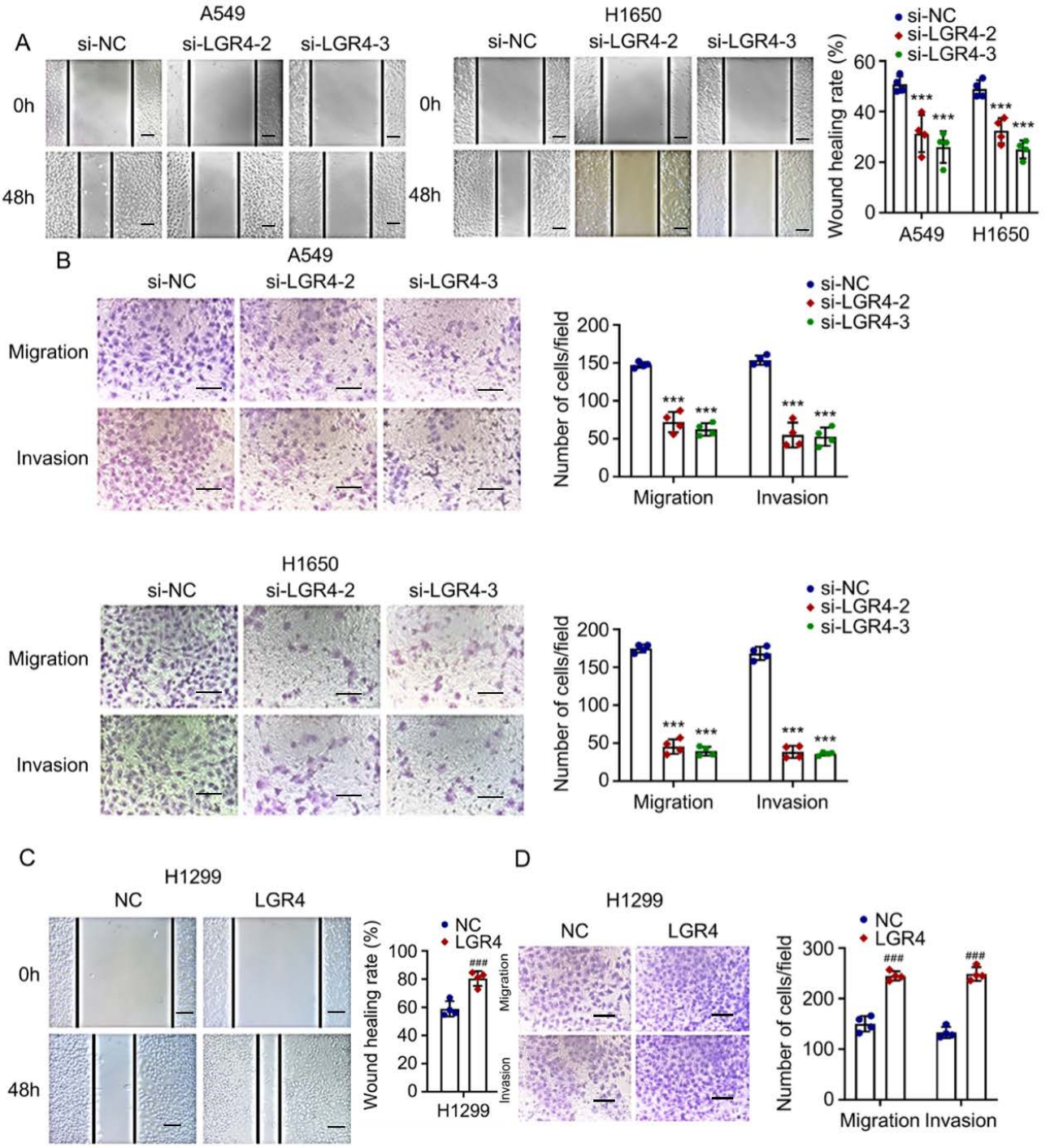

Fig. 5. LGR4 promotes LUAD cell migration and invasion. (A,B) Wound-healing and transwell assays demonstrating reduced migration and invasion in LGR4-knockdown A549 and H1650 cells (***$p < 0.001$ vs. control; scale bar = 100 μm). (C,D) LGR4 overexpression enhances wound closure, migration, and invasion in H1299 cells ($^{###}p < 0.001$ vs. control). Data are presented as mean ± SD from three independent experiments; scale bar = 100 μm; ***$p < 0.001$; $^{###}p < 0.001$.

havior [8]. Specifically, knockdown of LGR4 in A549 and H1650 cell lines resulted in marked reductions in cell proliferation, migration, and invasion, while overexpression in H1299 cells enhanced proliferative and metastatic potential. These findings were corroborated by *in vivo* xenograft models, where LGR4 knockdown significantly suppressed tumor growth, while overexpression accelerated tumor development, thereby underscoring its oncogenic potential.

Mechanistically, our data indicate that LGR4 promotes tumor progression at least in part through activation of the NF-κB signaling pathway [11,13,15,22]. GSVA and RNA-seq analyses showed that high LGR4 expression was

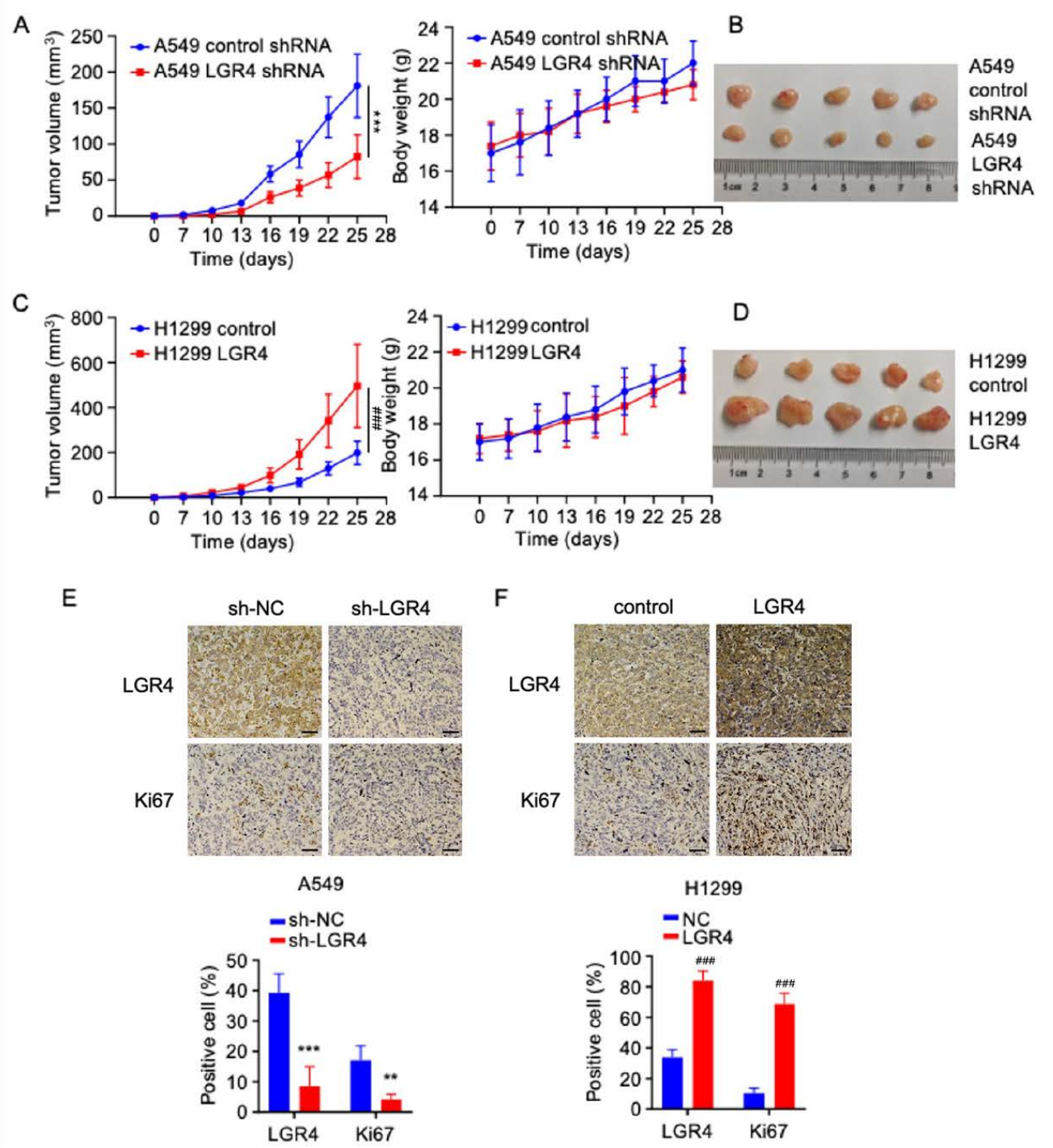

Fig. 6. LGR4 enhances tumor growth *in vivo*. (A–D) Xenograft tumor growth curves. LGR4 knockdown reduces tumor volume, whereas LGR4 overexpression increases tumor volume (***$p < 0.001$ vs. control; $^{###}p < 0.001$ vs. control) (cells injected: 1×10^6; body weights monitored). (E,F) Ki67 IHC (brown) on tumor sections. LGR4-knockdown tumors exhibit fewer Ki67$^+$ cells, whereas LGR4-overexpressing tumors show increased Ki67 staining (scale bar = 50 μm). Data are presented as mean ± SD; **$p < 0.01$ vs. control; ***$p < 0.001$ vs. control; $^{###}p < 0.001$ vs. control. shRNA, short hairpin RNA; Ki67, Ki-67 antigen.

associated with increased NF-κB pathway activity. This was further validated by the upregulation of phosphorylated proteins, including p-p65, p-IκBα, and p-IKKα/β, in LGR4-overexpressing cells, effects that were effectively reversed by the NF-κB inhibitor PDTC. Additionally, downstream effectors such as CCND1, MMP2 [24], and VEGF were elevated upon LGR4 overexpression but diminished following PDTC treatment, reinforcing the notion that NF-κB activation is a critical mediator of LGR4-driven oncogenic processes [25–27].

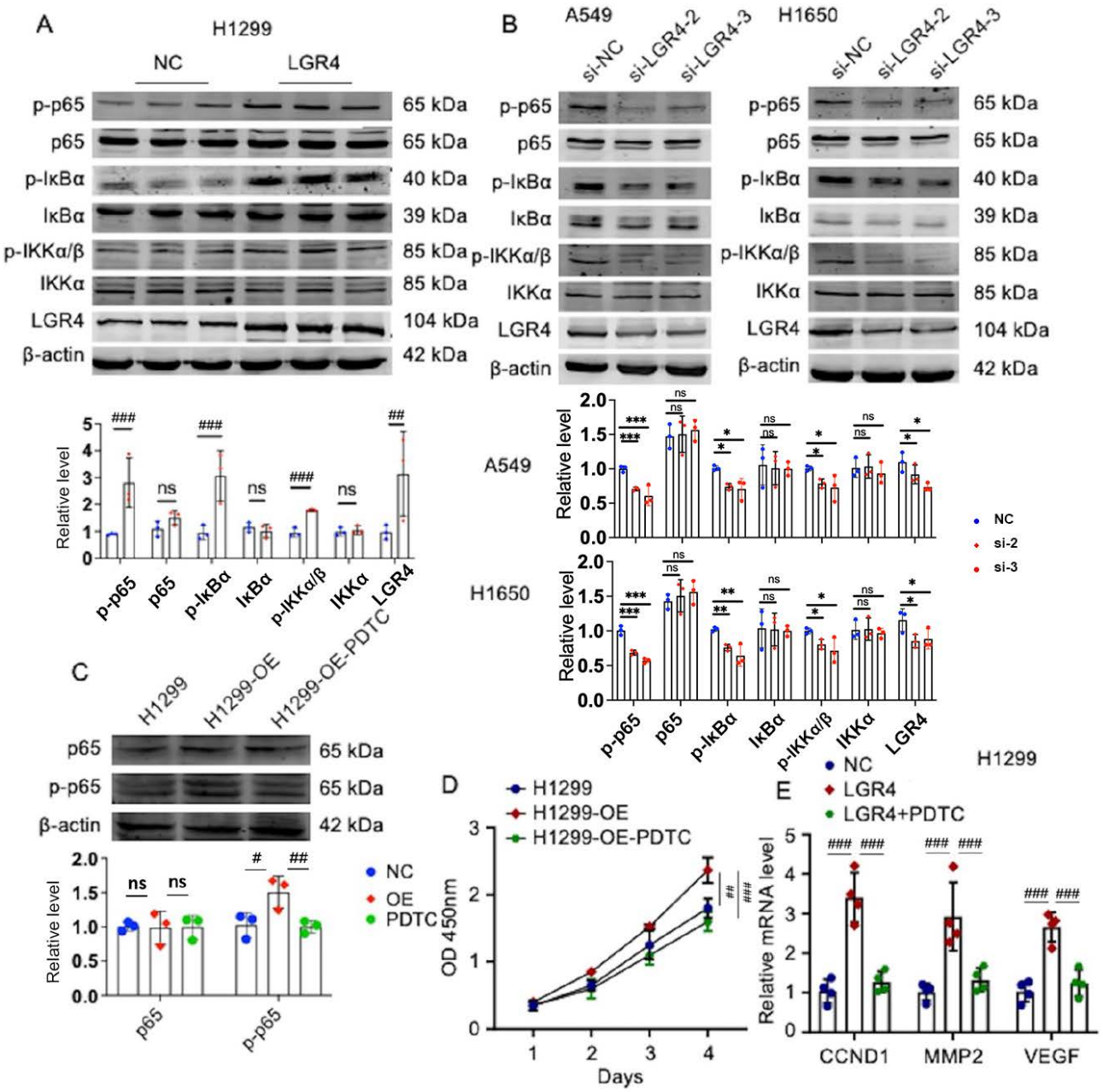

Fig. 7. LGR4 activates the NF-κB pathway to promote LUAD progression. (A,B) Western blot analysis showing increased phosphorylation of p65, IκBα, and IKKα/β with LGR4 overexpression, and decreased phosphorylation with LGR4 knockdown. Quantification of band intensities confirms these changes ($^{\#\#}p < 0.01$; $^{\#\#\#}p < 0.001$; $^{*}p < 0.05$; $^{**}p < 0.01$; $^{***}p < 0.001$). (C) Treatment with the NF-κB inhibitor PDTC reverses LGR4-induced NF-κB activation ($^{\#}p < 0.05$; $^{\#\#}p < 0.01$). (D) CCK-8 assay showing that PDTC reverses the pro-proliferative effect of LGR4 overexpression ($^{\#\#}p < 0.01$; $^{\#\#\#}p < 0.001$). (E) RT-qPCR analysis showing that *LGR4* overexpression upregulates *CCND1*, *MMP2*, and *VEGF*, whereas PDTC reverses this effect ($^{\#\#\#}p < 0.001$ vs. LGR4-OE without PDTC). Data are presented as mean $\pm$ SD from three independent assays; $^{*}p < 0.05$; $^{\#}p < 0.05$ vs. control; $^{**}p < 0.05$; $^{***}p < 0.001$; $^{\#\#}p < 0.01$; $^{\#\#\#}p < 0.001$. *CCND1*, cyclin D1; *MMP2*, matrix metalloproteinase 2; *VEGF*, vascular endothelial growth factor; PDTC, pyrrolidine dithiocarbamate; p65, p65 subunit of NF-κB; p-p65, phosphorylated p65 subunit of NF-κB; IκBα, inhibitor of κB alpha; p-IκBα, phosphorylated inhibitor of κB alpha; IKKα/β, IκB kinase alpha/beta; p-IKKα/β, phosphorylated IκB kinase alpha/beta.

Despite these compelling findings, several limitations need to be acknowledged. The precise molecular mechanism by which LGR4 activates NF-κB signaling remains incompletely understood, and it is plausible that LGR4 also engages other signaling pathways to promote tumorigenesis [28–30]. Moreover, the subcutaneous xenograft model employed in this study does not fully replicate the complex lung microenvironment, highlighting the need for further

validation using orthotopic models. Overall, our study provides novel insights into the role of LGR4 in lung adenocarcinoma and supports its potential utility as a prognostic biomarker and a therapeutic target.

Conclusion

This study identifies LGR4 as a critical driver promoter of LUAD progression. LGR4 is markedly overexpressed in LUAD and is associated with adverse clinical features. Functional experiments demonstrated that LGR4 promotes LUAD cell proliferation, migration, and invasion *in vitro* and accelerates tumor growth *in vivo*. Mechanistically, LGR4 activates the NF-κB signaling pathway, leading to upregulation of *CCND1*, *MMP2*, and *VEGF*, which drive tumorigenesis. Collectively, these findings suggest that LGR4 serves as a novel prognostic biomarker and potential therapeutic target in LUAD. Future research should elucidate the upstream regulation of LGR4 and explore targeted inhibition of the LGR4–NF-κB axis as a promising treatment strategy.

Availability of Data and Materials

All raw data and code are available from the corresponding author upon request.

Author Contributions

LL did most of the experiments and data analysis. KH, XK, ZL, and CY completed part of the experiment. WZ contributed to the study design and oversaw project management. LL wrote the original manuscript. All authors critically revised the manuscript for important intellectual content, approved the final version, and agreed to be accountable for all aspects of the work.

Ethics Approval and Consent to Participate

All animal and human experiments were conducted in compliance with the Chinese Animal License Regulations and were approved by the Animal Care and Use Committee of the Second Affiliated Hospital of Harbin Medical University (Animal Ethics Approval No. SYDW2023-087) and the Medical Ethics Committee (Human Ethics Approval No. KY2023-139).

Acknowledgment

Technical support from the Harbin Medical University Core Facility is gratefully acknowledged.

Funding

This study was supported by the Jieping Wu Medical Foundation (320.6750.2022-17-22).

Conflict of Interest

The authors declare no conflict of interest.

Supplementary Material

Supplementary material associated with this article can be found, in the online version, at https://doi.org/10.24976/Discov.Med.202537201.208.

References

[1] Luo J, Du X. A promising prognostic signature for lung adenocarcinoma (LUAD) patients basing on 6 hypoxia-related genes. Medicine. 2021; 100: e28237. https://doi.org/10.1097/MD.0000000000028237.

[2] Al-Dherasi A, Liao Y, Al-Mosaib S, Hua R, Wang Y, Yu Y, *et al*. Allele frequency deviation (AFD) as a new prognostic model to predict overall survival in lung adenocarcinoma (LUAD). Cancer Cell International. 2021; 21: 451. https://doi.org/10.1186/s12935-021-02127-z.

[3] Sun Y, Luo J, Chen Y, Cui J, Lei Y, Cui Y, *et al*. Combined evaluation of the expression status of CD155 and TIGIT plays an important role in the prognosis of LUAD (lung adenocarcinoma). International Immunopharmacology. 2020; 80: 106198. https://doi.org/10.1016/j.intimp.2020.106198.

[4] Cui Y, Fang W, Li C, Tang K, Zhang J, Lei Y, *et al*. Development and Validation of a Novel Signature to Predict Overall Survival in "Driver Gene-negative" Lung Adenocarcinoma (LUAD): Results of a Multicenter Study. Clinical Cancer Research: an Official Journal of the American Association for Cancer Research. 2019; 25: 1546–1556. https://doi.org/10.1158/1078-0432.CCR-18-2545.

[5] Antonia SJ, Villegas A, Daniel D, Vicente D, Murakami S, Hui R, *et al*. Overall Survival with Durvalumab after Chemoradiotherapy in Stage III NSCLC. The New England Journal of Medicine. 2018; 379: 2342–2350. https://doi.org/10.1056/NEJMoa1809697.

[6] Wang L, Luo R, Onyshchenko K, Rao X, Wang M, Menz B, *et al*. Adding liposomal doxorubicin enhances the abscopal effect induced by radiation/αPD1 therapy depending on tumor cell mitochondrial DNA and cGAS/STING. Journal for Immunotherapy of Cancer. 2023; 11: e006235. https://doi.org/10.1136/jitc-2022-006235.

[7] Tas SW, Bryant VL, Cook MC. Editorial: Non-canonical NF-κB signaling in immune-mediated inflammatory diseases and malignancies. Frontiers in Immunology. 2023; 14: 1252939. https://doi.org/10.3389/fimmu.2023.1252939.

[8] Besson A, Yong VW. Mitogenic signaling and the relationship to cell cycle regulation in astrocytomas. Journal of Neuro-oncology. 2001; 51: 245–264. https://doi.org/10.1023/a:1010657030494.

[9] Uekita T, Fujii S, Miyazawa Y, Iwakawa R, Narisawa-Saito M, Nakashima K, *et al*. Oncogenic Ras/ERK signaling activates CDCP1 to promote tumor invasion and metastasis. Molecular Cancer Research: MCR. 2014; 12: 1449–1459. https://doi.org/10.1158/1541-7786.MCR-13-0587.

[10] Yao L, Lai Y, Li H, Chen S, Yu X, Zhou N, *et al*. USP5 Deletion Inhibits KD Serum Induced-Human Coronary Artery Endothelial Cell Dysfunction by Regulating the NFATC1/TLR4-Mediated NF-κB Signaling Pathway in Kawasaki Disease. Inflammation. 2025. https://doi.org/10.1007/s10753-025-02276-7. (online ahead of print)

[11] Ranjbar A, Taghiloo S, Nozari P, Hedayatizadeh-Omran A,

Asgarian-Omran H. Effects of c-Kit Receptor, AKT, and NF-κB Inhibitors on Immune Evasion in Multiple Myeloma Cells. Iranian Journal of Allergy, Asthma, and Immunology. 2025; 24: 89–99. https://doi.org/10.18502/ijaai.v24i1.18024.

[12] Sharma N, Chandra Y, Andugulapati SB. Inhibition of MALT1 Protease Attenuates Hepatic Sinusoidal Obstruction Syndrome by Modulating NRF2/HO1 and NF-κB Pathway. Liver International: Official Journal of the International Association for the Study of the Liver. 2025; 45: e70050. https://doi.org/10.1111/liv.70050.

[13] Ding Y, Li X, Qi R, Su Y, Wang X. Chelerythrine-mediated targeting of NF-κB and Nrf2 pathways alleviates liver injury in a carbon tetrachloride-induced liver fibrosis mouse model. Histology and Histopathology. 2025; 18892. https://doi.org/10.14670/HH-18-892. (online ahead of print)

[14] Quan X, Miao Z, Han R, Deng R, Cao Y, Tian J, *et al*. Proteomic analysis reveals that Acalypha australis L. mitigates chronic colitis by modulating the FABP4/PPARγ/NF-κB signaling pathway. Journal of Ethnopharmacology. 2025; 345: 119585. https://doi.org/10.1016/j.jep.2025.119585.

[15] Mahjoubin-Tehran M, Rezaei S, Butler AE, Sahebkar A. Decoy oligonucleotides targeting NF-κB: a promising therapeutic approach for inflammatory diseases. Inflammation Research. 2025; 74: 47. https://doi.org/10.1007/s00011-025-02021-8.

[16] Liu Y, Zhang Y, Chen S, Zhong X, Liu Q. Effect of LGR4/EGFR signaling on cell growth and cancer stem cell-like characteristics in liver cancer. Cytokine. 2023; 165: 156185. https://doi.org/10.1016/j.cyto.2023.156185.

[17] Filipowska J, Cisneros Z, Varghese SS, Leon-Rivera N, Wang P, Kang R, *et al*. LGR4 is essential for maintaining β-cell homeostasis through suppression of RANK. Molecular Metabolism. 2025; 92: 102097. https://doi.org/10.1016/j.molmet.2025.102097.

[18] Fang Q, Ye L, Han L, Yao S, Cheng Q, Wei X, *et al*. LGR4 is a key regulator of hepatic gluconeogenesis. Free Radical Biology & Medicine. 2025; 229: 183–194. https://doi.org/10.1016/j.freeradbiomed.2025.01.025.

[19] Luo W, Tan P, Rodriguez M, He L, Tan K, Zeng L, *et al*. Leucine-rich repeat-containing G protein-coupled receptor 4 (Lgr4) is necessary for prostate cancer metastasis via epithelial-mesenchymal transition. The Journal of Biological Chemistry. 2017; 292: 15525–15537. https://doi.org/10.1074/jbc.M116.771931.

[20] Zeng Z, Ji N, Yi J, Lv J, Yuan J, Lin Z, *et al*. LGR4 overexpression is associated with clinical parameters and poor prognosis of serous ovarian cancer. Cancer Biomarkers: Section a of Disease Markers. 2020; 28: 65–72. https://doi.org/10.3233/CBM-191145.

[21] Ordaz-Ramos A, Rosales-Gallegos VH, Melendez-Zajgla J, Maldonado V, Vazquez-Santillan K. The Role of LGR4 (GPR48) in Normal and Cancer Processes. International Journal of Molecular Sciences. 2021; 22: 4690. https://doi.org/10.3390/ijms22094690.

[22] Deka K, Li Y. Transcriptional Regulation during Aberrant Activation of NF-κB Signalling in Cancer. Cells. 2023; 12: 788. https://doi.org/10.3390/cells12050788.

[23] Haselager MV, Eldering E. The Therapeutic Potential of Targeting NIK in B Cell Malignancies. Frontiers in Immunology. 2022; 13: 930986. https://doi.org/10.3389/fimmu.2022.930986.

[24] Wu CY, Liu Z, Luo WM, Huang H, Jiang N, Du ZP, *et al*. Downregulation of DIP2B as a prognostic marker inhibited cancer proliferation and migration and was associated with immune infiltration in lung adenocarcinoma via CCND1 and MMP2. Heliyon. 2024; 10: e32025. https://doi.org/10.1016/j.heliyon.2024.e32025.

[25] Gam DH, Park JH, Kim JH, Beak DH, Kim JW. Effects of *Allium sativum* Stem Extract on Growth and Migration in Melanoma Cells through Inhibition of *VEGF, MMP-2*, and *MMP-9* Genes Expression. Molecules (Basel, Switzerland). 2021; 27: 21. https://doi.org/10.3390/molecules27010021.

[26] Qu L, Wang JH, Du JX, Kang P, Niu XQ, Yin LZ. Use of nimotuzumab combined with cisplatin in treatment of nasopharyngeal carcinoma and its effect on expressions of VEGF and MMP-2. Clinical & Translational Oncology: Official Publication of the Federation of Spanish Oncology Societies and of the National Cancer Institute of Mexico. 2021; 23: 1342–1349. https://doi.org/10.1007/s12094-020-02522-4.

[27] Pai FC, Huang HW, Tsai YL, Tsai WC, Cheng YC, Chang HH, *et al*. Inhibition of FABP6 Reduces Tumor Cell Invasion and Angiogenesis through the Decrease in MMP-2 and VEGF in Human Glioblastoma Cells. Cells. 2021; 10: 2782. https://doi.org/10.3390/cells10102782.

[28] Gervas P, Molokov A, Babyshkina N, Zherebnova A, Choynzonov E, Cherdyntseva N. The frequency of known germline LGR4 missense variant in the ethnic groups of West Siberia. Molecular Biology Reports. 2024; 52: 42. https://doi.org/10.1007/s11033-024-10133-3.

[29] Xue M, Yang R, Li G, Ni Z, Chao Y, Shen K, *et al*. LGR4 Deficiency Aggravates Skin Inflammation and Epidermal Hyperplasia in Imiquimod-Induced Psoriasis. Immunology. 2025; 174: 213–225. https://doi.org/10.1111/imm.13873.

[30] Mehta P, Sharma A, Goswami A, Gupta SK, Singhal V, Srivastava KR, *et al*. Case report: exome sequencing identified mutations in the *LRP5* and *LGR4* genes in a case of osteoporosis with recurrent fractures and extraskeletal manifestations. Frontiers in Endocrinology. 2024; 15: 1475446. https://doi.org/10.3389/fendo.2024.1475446.